doi:10.3969/j.issn.1001-8352.2019.03.001

High Pressure Behavior of 4-Amino-3,7-dinitrotriazolo-[5,1,*c*] [1,2,4]triazine Crystal: a DFT Investigation*

YANG Dongfang①, ZHAO Guozheng①, LU Ming②
①Modern College of Humanities and Sciences of Shanxi Normal University (Shanxi Linfen, 041000)
②School of Chemical Engineering, Nanjing University of Science & Technology (Jiangsu Nanjing, 210094)

[**ABSTRACT**] The effect of external pressure on 4-amino-3,7-dinitrotriazolo-[5,1,*c*] [1,2,4] triazine (ADT) crystal in the pressure range of 0-130 GPa was investigated by the density functional theory (DFT) periodic calculation with LDA/CA-PZ function. With the increasing pressure, the volume of ADT crystal decreases while the energy increases. The topological analysis shows that the energy of hydrogen bonds increases as the pressure increases. At 81 GPa, hydrogen bonding between atoms O2 and H5 converts into covalent interaction. And the covalent interaction is formed between atoms N4 and H6. At 82 GPa, the interaction between atoms O2 and H5, N4 and H6 become hydrogen bonding. At 92 GPa, H6…N4 turns into a covalent bond, and there is s covalence interaction between the two atoms. The band gap decreases first and then increases with the increasing pressure.

[**KEYWORDS**] high pressure; ADT crystal; DFT; structure
[**CLASSIFICATION CODE**] TQ560; O64

4-氨基-3,7-二硝基三氮唑-[5,1,*c*][1,2,4]三嗪晶体高压行为的DFT研究

杨东芳① 赵国政① 陆 明②
①山西师范大学现代文理学院(山西临汾, 041000)
②南京理工大学化工学院(江苏南京, 210094)

[**摘 要**] 采用周期性密度泛函理论的LDA/CA-PZ方法研究0~130 GPa范围内压力对4-氨基-3,7-二硝基三氮唑-[5,1,*c*] [1,2,4]三嗪(ADT)晶体的影响。随压力的增加,ADT晶体的体积逐渐减小,能量逐渐升高。拓扑分析表明,氢键能随压力的升高而增大。81 GPa时,原子O2和H5间的氢键作用转化为共价作用,且原子N4和H6间形成共价作用;82 GPa时,原子O2与H5、N4与H6间的共价作用变为氢键作用;92 GPa时,氢键H6…N4转变为共价键,成键原子间存在强的共价作用。ADT晶体的带隙随压力的增加先降低再升高。

[**关键词**] 高压;ADT晶体;DFT;结构

Introduction

Nitrogen-rich energetic crystals, as a category of the high energetic density crystals, have been an important direction in the developing new energetic materials[1-3]. The nitrogen-rich energetic crystals exhibit high positive heats of formation and possess a large quantity of intermolecular and intramolecular hydrogen bonds which reduce the sensitivity[4]. And the gas generated by the detonations is more environmental than that of the traditional energetic materials.

In recent decades, a large number of new nitrogen-rich energetic crystals have been synthesized. Wu

* 收稿日期:2018-11-07
基金项目:山西师范大学现代文理学院基础研究重点项目(2018JCYJ03);山西师范大学现代文理学院教学改革创新项目(2019JG13)
第一作者:杨东芳(1992-),女,硕士研究生,主要从事含能材料高压行为研究。E-mail: ydfang1013@126.com
通信作者:赵国政(1985-),男,副教授,硕导,主要从事含能材料的计算模拟研究。E-mail: zhaoguozheng99@126.com

et al[5] improved the performance of 3-nitro-1,2,4-triazol-5-one (NTO) and 5,6,7,8-tetrahy-drotetrazolo[1,5-*b*][1,2,4]-triazine (TZTN) successfully by cocrystallizing NTO with TZTN in the ratio of 1∶1. Zhang et al[6] completed the synthesis of [2,2′-bi(1,3,4-oxadiazole)]-5,5′-dinitramide (ICM-101), a high-energy-density material. However, there are great limitations in the experimental study of high-pressure behavior of energetic crystals. Therefore, scientists start to study the high-pressure behavior of energetic crystals under extreme condition by the theoretical calculation, which contributes to understand the detonation mechanism[7-8]. Wu et al[9] studied the detonation and decomposition mechanism of 1,3,5-triamide-2,4,6-nitrobenzene (TATB) crystal at different decomposition temperatures and pressures by molecular dynamics simulation. Zhang et al[10] explored the structure, mechanics and vibration performance of 2,6-diamino-3,5-dinitropyrazine-1-oxide (LLM-105) in the range of 0-100 GPa by using density functional theory.

In 2016, David et al[11] synthesized the energetic crystal 4-amino-3,7-dinitrotriazole-[5,1,*c*][1,2,4]trazine (ADT) crystal. ADT (impact sensitivity of 29.0 J, friction sensitivity > 300 N) is less sensitive than RDX (impact sensitivity of 4.6 J, friction sensitivity of 157 N). In this paper, to further get more detailed insight into ADT crystal, the DFT was used to investigate the volume, total energy and band structure of ADT crystal within 0-130 GPa. And the hydrogen bonding was studied under different pressures by topology analysis.

1　Computational methods

Density functional theory (DFT) based on CASTEP code[12] was applied in the study with Vanderbilt-type ultrasoft pseudo-potentials. The local density approximation (LDA) with Ceperley-Alder exchange-correlation potential parameterized by Perdew and Zunder (CA-PZ)[13] was employed to the calculations on the ADT crystal. The electronic wave functions were obtained by using Pulay density-mixing scheme. Brillouin zone sampling was performed by using the Monkhorst-Pack scheme with *k*-point grid of 2×1×1. The experimental ADT crystal (CCDC 1481755)[11], used as initial structure, belongs to the monoclinic space group *Cc* with $a = 6.205$ Å, $b = 22.370$ Å and $c = 17.547$ Å as shown in Fig. 1.

The topology analysis was performed using Multiwfn[14] with the input files (.fchk) gained from Gaussian 09[15] using the functional B97-D at 6-311++G** level. The electron density (ρ_{BCP}) and its Laplacian ($\nabla^2\rho_{BCP}$) at the bond critical point (BCP), the total electron-energy density (H_{BCP}), the electron potential energy density (V_{BCP}) and the Lagrangain kinetic energy (G_{BCP}) were used to characterize the BCP. The relationships of these parameters were given by Equation (1):

$$\frac{1}{4}\nabla^2\rho = 2G_{BCP} + V_{BCP};$$
$$H_{BCP} = G_{BCP} + V_{BCP}。 \quad (1)$$

The hydrogen bond energy (E_H) was calculated

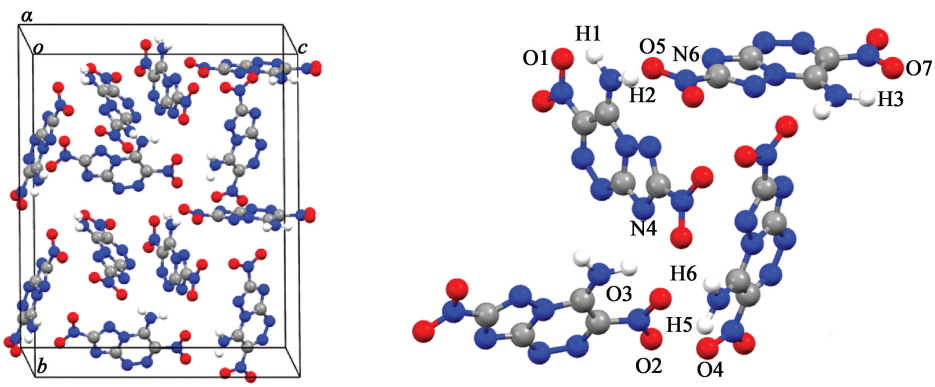

(a) crystal structure　　(b) atomic number

Fig. 1　Crystal structure and atomic number of ADT

as Equation(2):

$$E_H = \frac{1}{2}V_{BCP} \quad (2)$$

2 Results and discussion

2.1 Unit-cell volume and unit-cell angle

To visually illustrate the effect of hydrostatic pressure on molecular structures, the molecular configurations in ADT crystal under different pressures are displayed in Fig. 2. It is obvious that the molecular structures scarcely change below 80 GPa, because the external compression mostly squeezes out intermolecular space as the pressure increases to 80 GPa. When the hydrostatic pressure gets higher and higher, the planar conjugated structure deforms greatly, at the same time, there are remarkable rotations of the amino groups (—NH_2) and nitro groups (—NO_2) on the ring.

Fig. 3 describes the effect of pressure on the unit-cell angle and unit-cell volume of ADT crystal. It is clearly found that the unit-cell angle is greatly affected by hydrostatic pressure especially at 81, 82 and 92 GPa. The curve of unit-cell volume shows that the unit-cell volume decreases gradually, correspondingly, the crystal density increases with the increasing pressure. At low pressure, the distance between two molecules is large and the intermolecular forces are weak. Therefore, the unit-cell volume decreases fast at 0-10 GPa. Nevertheless, with the increase of hydrostatic pressure, the intermolecular repulsive forces become stronger gradually, hence the molecular conformation changes obviously. Fig. 4 presents the total energy of ADT crystal with the change of pressure. From Fig. 4, the total energy of ADT crystal rises with the increasing pressure, which means that the intermolecular interaction increases.

2.2 Topology analysis

The topology analysis proposed by Bader is an effective tool to obtain further insight into hydrogen bonds in ADT crystal by analyzing electron distribution in the 'atoms in molecules' (AIM) theory. The first necessary condition for the existence of hydrogen bond is that there is a bond critical point (BCP) for 'proton···acceptor' contact. The other criterion is that the value of

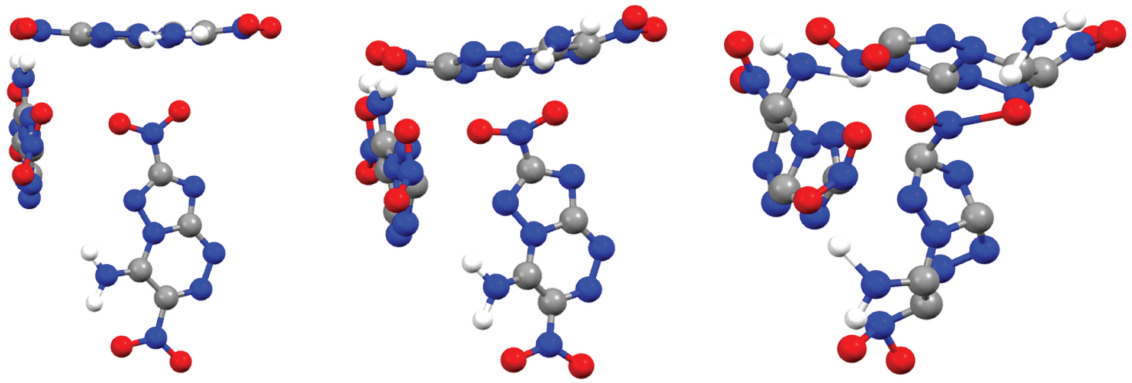

(a)0 GPa (b)80 GPa (c)130 GPa

Fig. 2 Variation trend of molecules in ADT crystal at different pressures

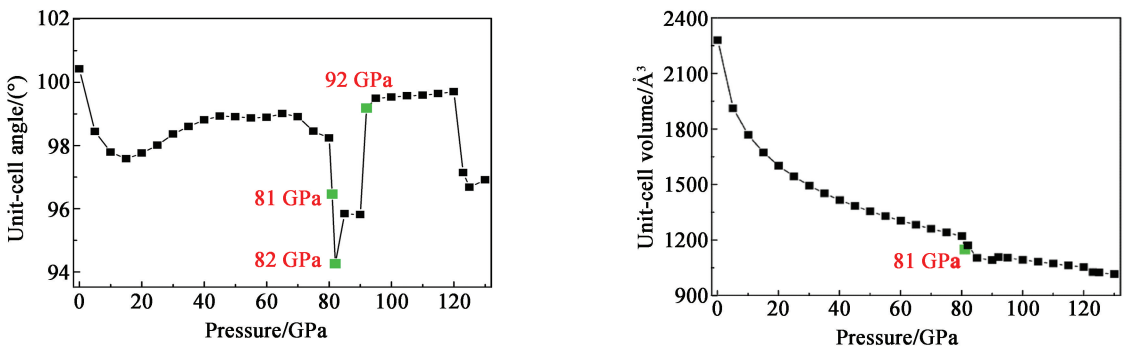

(a) Unit-cell angle (b) Unit-cell volume

Fig. 3 Unit-cell angle and unit-volume as a function of pressure for ADT crystal

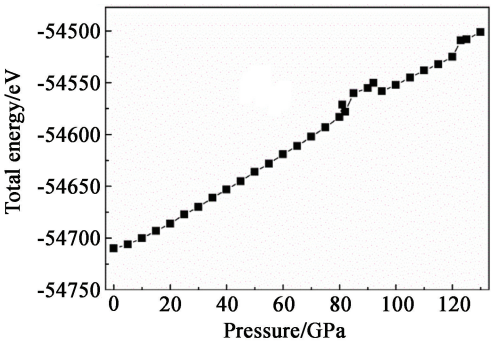

Fig. 4 Total energy as a function of pressure for ADT crystal

electron density at BCP (ρ_{BCP}) should be in the range of 0.002-0.040 a.u. and the corresponding Laplacian ($\nabla^2\rho_{BCP}$) value in the range of 0.024-0.139 a.u.. Hydrogen bond is classified by Rozas et al into three categories: if both $\nabla^2\rho_{BCP}$ and $H_{BCP}>0$, the H-bond is weak ($E_H \leqslant 50.2$ kJ/mol); if $\nabla^2\rho_{BCP}>0$ and $H_{BCP}<0$, the H-bond is medium ($50.2 < E_H < 100.5$ kJ/mol); however, if both $\nabla^2\rho_{BCP}$ and $H_{BCP}<0$, the H-bond is strong ($E_H > 100.5$ kJ/mol).

Herein , we discuss the intermolecular and intramolecular bond on the basis of the topological parameters and total electron density . Tab. 1 lists the calculated values of topology analysis and hydrogen bond energies for intermolecular hydrogen bonds under different hydrostatic pressures. It is clear from Tab. 1 that from 0 to 80 GPa, the hydrogen bond energies of H2…O5, H6…O3 and H5…O2 bonds increase with the increasing pressure and hydrogen bonds undergo a change from weak ($\nabla^2\rho_{BCP}>0$ and $H_{BCP}>0$) to medium ($\nabla^2\rho_{BCP}>0$ and $H_{BCP}<0$). Several distinct transformations in intermolecular hydrogen bonds occur within the pressure region of 80-130 GPa. At 81 GPa, both the electronic density and the Laplacian are positive in H2…N6, therefore, the H2…N6 forms which belongs to a weak hydrogen bond. At the same time, another new bond is formed by H6 and N4. The values $\nabla^2\rho_{BCP}<0$ and $H_{BCP}<0$ at the BCP show that the N4—H6 is a strong covalent bond and the bond energy reaches up to −595.99 kJ/mol. Since $\nabla^2\rho_{BCP}>0$ and $H_{BCP}<0$ at the BCP, the H5…O2 bond can be treated as a covalent bond, and what is more, the bond energy increases to −242.86 kJ/mol. Under 82 GPa, on the basis of the analysis of topology parameters and hydrogen bond energy, it can be concluded that H2…O5, H5…O2 and H6…O3 are considered as weak hydrogen bonds with the values $\nabla^2\rho_{BCP}>0$ and $H_{BCP}>0$, while the H6…N4 is regarded as a medium hydrogen bond with the values $\nabla^2\rho_{BCP}>0$ and $H_{BCP}<0$. When the pressure turns to 92 GPa, the $\nabla^2\rho_{BCP}$ and H_{BCP} at BCP

Tab. 1 Topology parameters and bond energy of intermolecular hydrogen bonds under different pressures

Pressure/GPa	Interaction H…Y	ρ_{BCP} (a.u.)	$\nabla^2\rho_{BCP}$ (a.u.)	V_{BCP} (a.u.)	G_{BCP} (a.u.)	H_{BCP} (a.u.)	E_H/(kJ·mol^{-1})
0	H2…O5	0.024	0.158	−0.032	0.036	0.004	−42.01
	H6…O3	0.017	0.077	−0.015	0.017	0.002	−19.69
	H5…O2	0.024	0.131	−0.025	0.029	0.004	−32.82
80	H2…O5	0.056	0.463	−0.120	0.122	−0.002	−157.53
	H6…O3	0.054	0.347	−0.092	0.090	−0.002	−120.77
	H5…O2	0.070	0.547	−0.154	0.145	−0.009	−202.16
81	H2…N6	0.029	0.184	−0.043	0.044	0.001	−56.45
	H5…O2	0.078	0.622	−0.185	0.170	−0.015	−242.86
	H6…N4	0.309	−0.014	0.454	0.053	−0.401	−595.99
82	H2…O5	0.043	0.328	−0.078	0.080	0.002	−102.40
	H5…O2	0.046	0.333	−0.080	0.081	0.001	−105.02
	H6…O3	0.042	0.239	−0.050	0.055	0.005	−65.64
	H6…N4	0.050	0.372	−0.102	0.097	−0.005	−133.90
92	H2…N6	0.023	0.134	−0.028	0.031	0.003	−36.76
	H5…O2	0.047	0.329	−0.081	0.081	0	−106.33
	H6…N4	0.153	−0.730	−0.419	0.118	−0.301	−550.04

in H2⋯N6 and H5⋯O2 bonds are positive or zero which elucidates that H2⋯N6 and H5⋯O2 bond are classified as weak hydrogen bonds. Furthermore, the hydrogen bond interaction between H6 and N4 changes into much stronger covalent interaction. The $\nabla^2\rho_{BCP}$ and H_{BCP} of H6—N4 bond at the BCP are lower than zero and the E_H of H6—N4 bond is as high as −550.04 kJ/mol.

Tab. 2 depicts the topology parameters and hydrogen bond energies for intramolecular hydrogen bonds under various pressures. The topology parameters $\nabla^2\rho_{BCP}$ and H_{BCP} in H1⋯O1, H5⋯O4 and H3⋯O7 bonds are positive within the pressure region of 0-130 GPa, except that at 82 and 123 GPa. From 81 to 82 GPa, the H3⋯O7 bond turns from weak ($\nabla^2\rho_{BCP}>0$, $H_{BCP}>0$) to medium strength H-bond ($\nabla^2\rho_{BCP}>0$, $H_{BCP}<0$).

2.3 Band structure

The self-consistence band structures, basing on equilibrium crystal structures under different pressures, are illustrated in Fig. 5, in which only the energetic band structure from −0.75 to 2.00 eV is appeared. As shown in Fig. 5, when the pressure is lower than 81 GPa, the energy bands including conduction bands and valence bands are almost flat because the ADT crystal is a molecular crystal and the intermolecular interactions are weak in ADT crystal. With the augment of pressure, the energy bands fluctuate obviously and shift to lower energy region. In the pressure range of 81-92 GPa, the widths of conduction and valence bands broaden which are caused by transformations of configuration and intermolecular interactions. When the pressure is above 123 GPa, the energy bands shift obviously to higher energy region compared with those at 92 GPa.

3 Conclusions

In this study, periodic DFT calculations with LDA/CA-PZ function were performed to explore the effect of external pressure on ADT crystal in the range of 0-130 GPa. In the whole pressure, the volume of ADT crystal decreases gradually and the energy increases monotonously.

Overall, the hydrogen bond energy (E_H) increases as the pressure increases and hydrogen bonding in ADT crystal becomes stronger under high pressure. At 81 GPa, there is a covalent interaction between atoms N4 and H6. The hydrogen bonding between atoms H5 and O2 converts into covalent interaction and the E_H reaches −202.16 kJ/mol. At 82 GPa, the E_H of H5⋯O2 decreases to −102.40 kJ/mol and belongs to a hydro-

Tab. 2 Topology parameters and bond energy of intramolecular hydrogen bonds under different pressures

Pressure/GPa	Interaction H⋯Y	ρ_{BCP} (a.u.)	$\nabla^2\rho_{BCP}$ (a.u.)	V_{BCP} (a.u.)	G_{BCP} (a.u.)	H_{BCP} (a.u.)	E_H/(kJ·mol^{-1})
0	H1⋯O1	0.023	0.125	−0.023	0.027	0.001	−30.19
	H3⋯O7	0.023	0.124	−0.023	0.027	0.004	−30.19
	H5⋯O4	0.023	0.124	−0.023	0.027	0.004	−30.19
80	H1⋯O1	0.042	0.264	−0.057	0.061	0.004	−74.83
	H3⋯O7	0.044	0.313	−0.073	0.076	0.003	−95.83
	H5⋯O4	0.041	0.258	−0.059	0.062	0.003	−77.45
81	H1⋯O1	0.038	0.241	−0.052	0.056	0.004	−68.26
	H3⋯O7	0.046	0.296	−0.073	0.074	0.001	−95.83
	H5⋯O4	0.023	0.127	−0.027	0.029	0.002	−35.44
82	H1⋯O1	0.053	0.394	−0.097	0.098	0.001	−127.34
	H3⋯O7	0.070	0.575	−0.162	0.153	−0.009	−212.67
	H5⋯O4	0.036	0.239	−0.053	0.057	0.004	−69.58
92	H1⋯O1	0.040	0.256	−0.059	0.062	0.003	−77.45
	H3⋯O7	0.052	0.364	−0.091	0.091	0.000	−119.46
	H5⋯O4	0.046	0.301	−0.070	0.072	0.002	−91.89

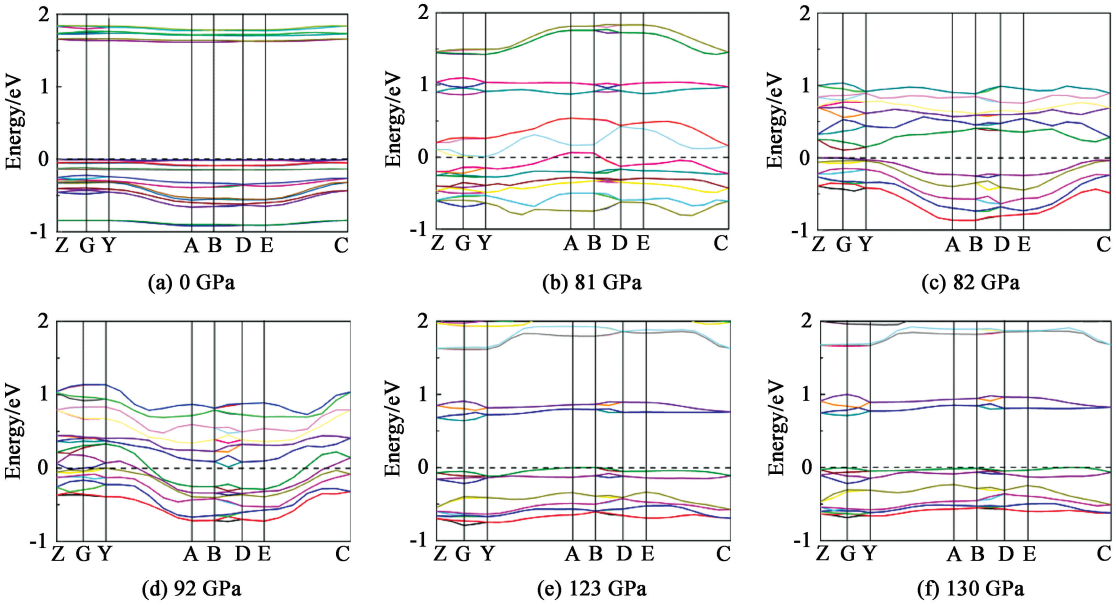

Fig. 5　Self-consistence band structures of crystalline ADT under different pressures. The Fermi energy is shown as a dashed horizontal line

gen bond. Meanwhile, the covalent interaction between atoms N4 and H6 transfers into hydrogen bond interaction. When the pressure further increase to 92 GPa, there exists a covalent effect between the two bonding atoms N4 and H6 and the E_H up to −643.25 kJ/mol.

The energy bands fluctuate obviously at 81, 82 and 92 GPa, respectively. With the increasing pressure, the band gap decreases first and then increases.

References

[1] CAO W L, DING Z M, HANG X J, et al. Theoretical study of a series of 4, 4′-azo-1*H*-1, 2, 4-triazol-5-one based nitrogen-rich salts as potential energetic compounds [J]. RSC Advances, 2018, 8(42): 23805-23816.

[2] LI W B, HUANG X L, BAO K, et al. A novel high-density phase and amorphization of nitrogen-rich 1H-tetrazole (CH_2N_4) under high pressure [J]. Scientific Reports, 2017, 7: 39249-39258.

[3] MA P, PAN Y, JIANG J C, et al. Molecular dynamic simulation and density functional theory insight into the nitrogen rich explosive 1,5-diaminotetrazole (DAT) [J]. Procedia Engineering, 2018, 211: 546-554.

[4] KLAPÖTKE T M, WITKOWSKI T G. Nitrogen-rich energetic 1,2,5-oxadiazole-tetrazole-based energetic materials [J]. Propellants, Explosives, Pyrotechnics, 2015, 40(3): 366-373.

[5] WU J T, ZHANG J G, LI T, et al. A novel cocrystal explosive NTO/TZTN with good comprehensive properties [J]. RSC Advances, 2015, 5(36): 28354-28359.

[6] ZHANG W Q, ZHANG J H, DENG M C, et al. A promising high-energy-density material [J]. Nature Communications, 2017, 8: 181.

[7] ZHANG L Y, LIU H, ZHENG W F, et al. DFT study on the structure and properties of difluoramino derivatives of CL-20 [J]. Explosive Materials, 2018, 47(3): 7-13.
张路遥, 刘卉, 郑文芳, 等. CL-20 二氟氨基衍生物结构与性能的 DFT 研究 [J]. 爆破器材, 2018, 47(3): 7-13.

[8] ZHU J, XU D, WANG P C. Computational study on the chemical structure and explosive properties of 2,6-bis(dinitromethylidene)-1,3,4,5,7,8-hexanitrododecahydrodiimidazo[4,5-b:4′,5′-e] pyrazine [J]. Explosive Materials, 2018, 47(3): 1-6.
祝洁, 许登, 王鹏程. 2,6-双(二硝基亚甲基)-1,3,4,5,7,8-六硝基十二氢二咪唑[4,5-b:4′,5′-e]吡嗪分子结构及性能的理论计算 [J]. 爆破器材, 2018, 47(3): 1-6.

[9] WU Q, CHEN H, XIONG G L, et al. Decomposition of a 1,3,5-triamino-2,4,6-trinitrobenzene crystal at decomposition temperature coupled with different pressures: an ab initio molecular dynamics study [J]. The Journal of Physical Chemistry C, 2015, 119(29): 16500-16506.

[10] ZONG H H, ZHANG L, ZHANG W B, et al. Structural, mechanical properties, and vibrational spectra of LLM-105 under high pressures from a first-principles study [J]. Journal of Molecular Modeling, 2017, 23: 275.

(下转第12页)

Journal of the American Oil Chemists' Society, 1928, 5(11), 317-326.

[10] BOURBIGOT S, CHLEBICKI S, MAMLEEV V. Thermal degradation of cotton under linear heating[J]. Polymer Degradation & Stability, 2002, 78(1):57-62.

[11] ZHU P, SUI S Y, WANG B, et al. A study of pyrolysis and pyrolysis products of flame-retardant cotton fabrics by DSC, TGA, and PY-GC-MS [J]. Journal of Analytical and Applied Pyrolysis, 2004, 71(2):645-655.

[12] WANG Q S, SUN J H, GUO S. Spontaneous combustion identification of stored wet cotton using a C80 calorimeter [J]. Industrial Crops and Products, 2008, 28(3):268-272.

[13] ZHAO X J, XIAO H H, WANG Q S, et al. Study on spontaneous combustion risk of cotton using a microcalorimeter technique [J]. Industrial Crops and Products, 2013, 50:383-390.

[14] CEYLAN Ö, VAN LANDUYT L, RAHIER H, et al. The effect of water immersion on the thermal degradation of cotton fibers [J]. Cellulose, 2013, 20(4): 1603-1612.

[15] WAKELYN P J, HUGHS S E. Evaluation of the flammability of cotton bales [J]. Fire and Materials, 2002, 26(4/5):183-189.

[16] 包任烈, 张永丰, 顾海昕, 等. 棉花自燃风险性的热分析研究 [J]. 消防科学与技术, 2012, 31(1):100-103.
BAO R L, ZHANG Y F, GU H X, et al. The research of cotton's self-ignition risk by thermal analysis[J]. Fire Science and Technology, 2012, 31(1):100-103.

[17] ALONGI J, CAMINO G, MALUCELLI G. Heating rate effect on char yield from cotton, poly(ethylene terephthalate) and blend fabrics [J]. Carbohydrate Polymers, 2013, 92(2):1327-1334.

[18] 张成梁, 冯显英, 杨丙生, 等. 基于相对湿度的棉花回潮率在线检测 [J]. 沈阳工业大学学报, 2013,35(4):445-450.
ZHANG C L ,FENG X Y, YANG B S, et al. Online detection of cotton moisture regain based on relative humidity[J]. Journal of Shenyang University of Technology, 2013,35(4):445-450.

[19] Recommendations on the transport of dangerous goods: manual of tests and criteria [M]. New York and Geneva: United Nations, 2015.

[20] 全国塑料标准化技术委员会. 塑料燃烧性能试验方法 闪燃温度和自燃温度的测定:GB/T 9343—2008 [S]. 北京:中国标准出版社,2008.

[21] 潘田震, 邵学民. 对一起棉花堆垛自燃火灾的调查 [J]. 消防科学与技术, 2004, 23(6): 604-605.

[22] 顾海昕, 张永丰, 曹丽英. 不同温湿度下棉花分解气体测试实验研究[C]//2013 中国消防协会科学技术年会论文集. 合肥,2013:298-304.

[23] HAGEN B C, FRETTE V, KLEPPE G, et al. Onset of smoldering in cotton: effects of density [J]. Fire Safety Journal, 2011, 46(3):73-80.

(上接第6页)

[11] PIERCEY D G, CHAVEZ D E, SCOTT B L, et al. An energetic triazolo-1,2,4-triazine and its N-oxide [J]. Angewandte Chemie, 2016, 128: 1-5.

[12] CLARK S J, SEGALL M D, PICKARD C J, et al. First principles methods using CASTEP [J]. Zeitschrift für Kristallographie: Crystalline Materials, 2005, 220(5/6): 567-570.

[13] CEPERLEY D M, ALDER B J. Ground state of the electron gas by a stochastic method [J]. Physical Review Letters, 1980, 45(7): 566-569.

[14] LU T, CHEN F W. Multiwfn: a multifunctional wavefunction analyzer [J]. Journal of Computational Chemistry, 2012, 33(5): 580-592.

[15] FRISCH M J, TRUCKS G W, SCHLEGEL H B, et al. Gaussian 09[CP]. Revision A. 02. Wallingford CT: Gaussian Inc., 2009.